Beam tests of ATLAS SCT silicon strip detector prototypes; an overview of recent results

M. Vos [a,1], M. D'Onofrio [b], J.E. Garcia Navarro [a], G.F. Moorhead [c,*]
for the ATLAS SCT collaboration

[a] *IFIC, U. Valencia/CSIC, Spain*
[b] *University of Geneva, Switzerland*
[c] *University of Melbourne, Australia*

Abstract

In recent years, ATLAS Semiconductor Tracker (SCT) silicon strip detector modules have been routinely tested in beam tests at the H8 beamline of the CERN SPS and in the $\pi 2$ beamline of the KEK PS. Measurements have established the tracking performance of prototypes of the final design of the various SCT geometrical module types under different operating conditions. Tests of irradiated modules have allowed estimation of the performance after 10 years of operation in the LHC. In this article, the test beam setup and methodology is described and an overview of the most important results presented.

1 Introduction

Prototype ATLAS Semiconductor Tracker (SCT) modules have been tested several times a year at the H8 beamline of the Super Proton Synchrotron (SPS) at CERN. In 1999 and 2000, additional tests were carried out at the $\pi 2$ beamline at KEK's 12 GeV Proton Synchrotron in Tsukuba, Japan. In H8 several secondary beam types are possible, the most commonly used for this work being 180 GeV charged pions. In KEK beam tests a 4 GeV pion beam is used.

* Corresponding author
Email address: Gareth.Moorhead@cern.ch (G.F. Moorhead).
[1] in collaboration with Universiteit Twente, The Netherlands

Modules are tested in an inline array along the beam axis, typically with 10 or 12 modules present. Modules of all four SCT geometries have been tested: rectangular barrel modules and the three types of wedge-shaped end-cap modules. Of particular interest is the study of the evolution of the module performance with irradiation at levels expected during the lifetime of the experiment in the LHC. To this end, many modules have been irradiated up to fluences of $3 \cdot 10^{14} p/cm^2$ in the CERN PS T7 proton irradiation facility [1].

A beam test experiement typically consisted first of a detailed electrical characterisation and optimisation of the front-end response of the modules after installation at operating conditions. Beam data was then taken for around one week during which the operating parameters of interest were scanned. In the binary readout scheme adopted by the SCT the signal from each strip is discriminated on the module at acquisition, necessitating a fine-grained scan of the threshold to determine the collected charge distribution. The charge collection efficiency is characterised by the median of this charge distribution.

Operating conditions of interest included particle incidence angle, silicon detector bias voltage, magnetic field, and the operating modes of the front-end integrated circuits. These were studied by performing nested scans of the operating parameter and the discriminator threshold. The effect of a strong magnetic field was tested by inserting the complete setup in the superconducting 1.7 T Morpurgo magnet available at H8. The deviation of the charge carriers due to the Lorentz effect has been studied in detail yielding a precise measurement of the Lorentz angle.

Detailed results of beamtests have been published in internal notes and conference proceedings [2–10]. A detailed description of beamtests prior to 1999 can be found in [11–15].

In this article, an overview of the beamtest methodology and results is presented. In the first section, the experimental setup used in recent years is described. In section 3, the off-line pre-processing steps applied to the raw data are outlined. In the same section the most important measurements of the single-module tracking performance - efficiency, noise occupancy, spatial resolution - are defined. An overview of results for recent SCT prototype and early production modules is given in section 4. A concluding section (5) summarizes the findings.

2 Setup

The H8 test area at CERN receives a secondary beam from the 400-450 GeV SPS. Several particle types and ranges of beam energies are available. The

standard beam for tests of SCT modules is 180 GeV charged pions with a minor contamination of muons. The beam in the $\pi 2$ line of the 12 GeV Proton Synchrotron at KEK is 3-4 GeV pions.

The setup used in recent years is depicted in figure 1. The particular arrangement illustrated corresponds to August 2002 at CERN. It consists of a scintillator trigger, a beam telescope and a refrigerated chamber containing the modules under test.

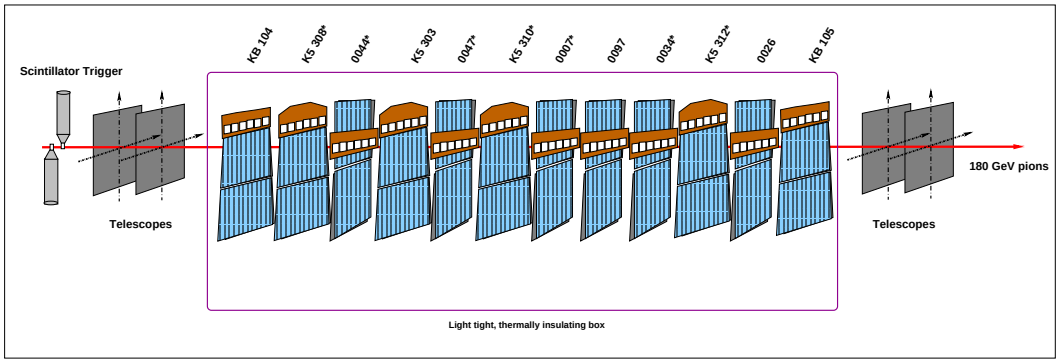

Fig. 1. *Arrangement of SCT prototype modules in the H8 beamline during the August 2002 beamtest.*

The telescope and modules under test are mounted on a granite table sitting on a trolley on a set of rails such that it can be inserted into the active volume of the magnet. The magnetic field points vertically downward, i.e. parallel to the readout strips of the detectors in the standard module configuration in emulation of the relative orientation of tracks and field with respect to strips in the SCT barrel.

The most important systems - binary readout and control, beam telescope, trigger and cooling - are discussed in the following sections.

2.1 Trigger

Two scintillator detectors read out by Photo Multiplier Tubes are used to detect the passage of beam particles and thence trigger the readout system. The trigger signal timing jitter is around 1-2 nanoseconds.

In ATLAS the readout of the detectors will be synchronized with the bunch crossings of the LHC. The SCT timing will be carefully optimized to ensure that the signal is sampled at the peak of the charge response curve. In most beam tests, however, the beam and readout clock are not synchronized [2] . The

[2] In certain periods the SPS has been operated with an "LHC-like" bunch structure which has been used to test SCT modules under more stringent timing conditions.

beam particles, and the trigger, arrive with a random phase with respect to the 40 MHz readout clock. Since electronics designed for the for LHC has typically a very short rise time comparable to the 25 nanosecond clock period, this random arrival time would have a severe effect on the apparent performance. Therefore the time between the raw trigger from the scintillators and the next rising edge of the clock was measured using a high-resolution Time to Digital Converter (TDC) [3], allowing the performance dependence on trigger phase to be evaluated off-line.

The acceptance of the scintillators is typically $2\times2cm^2$, large enough to contain typical beam spots and comparable in size to the acceptance of the beam telescope. The SCT modules have a sensitive area of $6 \times 12cm^2$.

2.2 Beam telescope

The telescope is used to reconstruct independently the trajectories of beam particles to high precision. It consists of four modules mounted in pairs on either side of the thermal enclosure of the modules under test. The telescope and the modules are mounted on the same massive granite table to ensure the mechanical rigidity of the system.

Each of the four telescope modules consists of a two perpendicular silicon micro-strip sensors with a strip pitch of $50\mu m$. The detectors are read out by VA2 analog multiplexed readout chips with around $1\mu s$ peaking time. The spatial resolution obtained is well below $5\mu m$.

IRAM flash ADC cards measure the signal from each telescope module. A DSP on the IRAMs subtracts pedestals and applies a clustering algorithm, significantly reducing the data volume. The total dead time of this system, $\sim 13ms$, is the dominant factor in the event rate.

In addition to the telescope, one of the SCT modules is usually read out as an anchor module. This means the module remains at a fixed threshold and bias voltage optimized for high efficiency and low noise throughout the scans. In addition to providing an extra measurement position inside the array of modules under test, the anchor module provides an efficiency reference. The requirement that at least one of the two sensor planes of the anchor module is efficient effectively reduces residual inefficiencies due to readout glitches, badly reconstructed tracks and tracks with a large deflection due to multiple scattering in the setup.

In this case the readout clock was synchronized to the accelerator RF bunches using the LHC timing distribution system.

[3] CAEN model V488

In the KEK beamtests, where the beam energy is much lower, multiple scattering is a serious problem. Therefore, the telescope and binary modules are interleaved in the same volume. The intermediate telescope measurement efficiently removes tracks that suffer a large deflection.

2.3 Binary readout and control

SCT modules are powered, controlled and readout by a suite of custom VME modules.

The clock and control module (CLOAC) provides a common 40 MHz system clock that is distributed to all modules and to the readout system. It is also used to distribute common "short" commands - resets and level-one triggers - to the modules and to the readout system.

A slow command generator module (SLOG) assembles and sends slow commands specific to each module. These are used to configure the ABCD3T front-end readout ASICs, loading the configuration register, the settings for the DACs that control the front-end currents and the threshold, and the trim and mask registers. The slow commands are merged with the common fast commands and distributed independently to each module on a data link along with the common clock. Each SLOG fans out clock and control signals to six modules.

Each module is equipped with twelve ABCD3T readout ASICs, connected in a daisy-chain. Two of these chips are connected to readout links normally used to send the binary hit information from each side of the module in digital data packets. The"MuSTARD" VME module receives, decodes and buffers this data from six modules, i.e., from twelve readout links. The SCT redundancy schemes, where all data is read through either one of the two data links, or when any individual chip which may have failed is bypassed in the daisy-chain, is fully supported.

The ABCD3T fully implements the digital pipeline and multiple event buffer schemes required by the high trigger rate and long trigger latency of ATLAS. After a level-one accept (L1A), the binary data corresponding to that binary clock phase is shifted from the pipeline to the event readout buffer along with the data from one preceding and one succeeding clock phase. The digital data packet from one event thus contains the hit patterns for all strips for three successive time bins. Several data compression modes are implemented with increasing degree of severity depending on the occupancy of the three time bins. In the beam test, one of the less severe modes, where any hit in the central bin results in output data, is used. This provides more timing information as well as allowing the more severe modes to be simulated off-line.

In the LHC all signals to and from the SCT will be carried on optical fibres, and converted to electrical signals at the module. In the beam tests, optical readout was not available. Instead, the LVDS electrical signals were buffered at the module and transmitted on 25 m shielded twisted-pair cables.

Custom VME modules are also used to provide ASIC power, slow controls and the detector bias high-voltage. These modules are installed in a separate VME crate.

2.4 Module calibration

A full characterisation of the module front-end parameters such as gain and noise is made in situ prior to the beam test using the ABCD3T's in-built calibration circuit. A voltage step through the calibration capacitor (Ccal) results in accumulated charge being injected into the front-end of the chip at the place of the charge collected in the silicon detector. Nested scans of threshold, calibration strobe line and calibration charge amplitude are performed. A complementary error function is fitted to the threshold "s-curve" for each strip for each calibration charge setting, yielding values of the 50% point efficiency (vt_{50}) and output noise. To obtain the response curve, the parameterisation of the function relating input charge to discriminator threshold setting, a multi-parameter fit to the set of vt_{50} points is performed. The gain and offset for each strip are determined from these response curves, and the input noise calculated by dividing the output noise measured at 2 fC by the gain. In this procedure, the effective corrected calibration charge is determined from the ABCD3T specification for the calibration capacitor combined with a measurement of the process capacitance values obtained from samples of each chip batch.

The ABCD3T implements trim settings to permit adjustment of the threshold for each strip to minimise threshold spread. The optimisation of these settings is a lengthy procedure also carried out before the final response is measured. More details on the estabilished module calibration can be found in [16].

In addition to the standard electrical procedure described, further optimisation is required for irradiated modules, as described in [17]. Modelled as a transimpedance amplifier with a bipolar input transistor, the front-end circuit of unirradiated ASICs have nominal values for collector (pre-amplifier) and shaper currents of 220 μA and 30 μA respectively. As a consequence of the β factor degradation, the optimum values of these currents decrease with irradiation. Two 5-bit DACs are thus implemented in the ABCD3T in order to adjust the pre-amplifier and shaper currents[18]. Each chip must be independently optimised, with typical values for irradiated modules around 120 or

140 μA for the input transistor current and 27 or 30 μA for the shaper bias.

This procedure, the so called current scan, is typically made as first step of the electrical tests following the irradiation and subsequent annealing, prior to the beam test. In 2002 beam tests of irradiated modules with different current configurations were performed to study the variation of signal-to-noise with respect to preamplifier and shaper current.

Furthermore, a degradation in digital timing performance has been observed with irradiation. It was found that the number of slow channels can be significantly reduced by increasing the analog voltage, V_{cc}, supplied to the chips. Setup effects such as these are avoided by running the final response curve calibration in-situ, immediately before taking beam data. For example, the temperature differences of the chips may also have a 5 % effect on the noise measurement [2].

2.5 Cooling

The devices under test are held in a light-tight thermally insulating box. The box is flushed with cold nitrogen to ensure a dry atmosphere. Each of the modules is contained in its own aluminium test box. The module boxes are equipped with mounting points and cooling contacts similar to those to be employed in ATLAS. The modules are cooled individually by a water-ethanol (60:40) mixture at -15^o C flowing through a cooling pipe in the module box, immediately under the cooling point, removing the some 7 Watts of dissipated power.

The resulting hybrid temperatures, measured at the thermistor mounted on the electronics hybrid of the module, are monitored continuously. Hybrid temperatures range between -5 and 5^o C. The differences between modules are small compared to the variation across the hybrid and should not lead to significant differences in electronics noise. The leakage current of irradiated detectors is in the range from 1 to 3 mA, depending on the bias voltage and fluence. SCT modules are typically irradiated to a reference value of $3 \times 10^{14} p/cm^2$, regarded as the worst case to be expected plus a 50 % margin. The non-irradiated modules have currents of the order of $1 \mu A$.

3 Off-line & Analysis

During the beam test, data from all sub-systems - telescope modules, SCT binary modules, TDC - are assembled into events and written to data files.

To facilitate the analysis, these raw data are processed off-line into summary files, traditionally known as DSTs (Data Summary Tapes). The summary files present the data in an easily accessible n-tuple format. Off-line processing includes the internal alignment of telescope and module planes and the reconstruction of tracks using the measurements of the beam telescope.

3.1 Alignment

The beam telescope provides four very precise measurements in two perpendicular space coordinates. The reconstruction of the track and the interpolation to the plane of the prototype require a precise knowledge of the relative alignment of all detectors in the setup.

The positions of telescope and SCT modules, though stable, are only approximately fixed by the mounting frames. A precision measurement of the relative alignment of all planes is obtained using the tracks in a large number (~ 10000) of events. The alignment procedure optimises the alignment error, i.e., minimises the residuals, by iteratively varying the alignment parameters.

As a first step in the alignment procedure, the position of the global telescope frame is fixed by identifying X and Y axes with the coordinates measured by the first two telescope frames and the Z-axis with the beam. Once the global system is defined, the remaining telescope planes are aligned by minimising the distance of their hits to tracks reconstructed from the outer two modules. At this stage only two space points are used to define a track. Ambiguities due to noise hits are effectively avoided by rejecting events in which all four planes under consideration do not have exactly one hit. After the internal alignment of the telescope, full 3 or 4 space point information from the telescope can be used to reconstruct tracks projected through the modules under test. The alignment parameters of each of the two planes of the test modules are varied until the difference between the extrapolated track position and the measurement by the plane converges to a minimum.

When a magnetic field is applied, the assumption of straight tracks is no longer valid. However, applying the alignment procedure on data taken in the magnetic field yields good results as the effect of the magnetic field is absorbed in the position of the planes.

SCT modules are composed of four separate silicon wafers mounted in pairs as back-to-back planes rotated with respect to each other at a stereo angle of 40 milliradians. When information from the two planes are combined, a space point with high resolution across the nearly parallel strips and low-rsolution along the strips is formed. In the beam test analysis, the stereo planes are aligned independently. When the beam, which is considerably narrower than

the silicon detectors, is contained within a single silicon wafer of each plane, the alignment procedure is insensitive to the module assembly precision, i.e. the wafer-to-wafer and the front-to-back alignment.

The alignment procedure is repeated each time the setup is accessed and whenever the magnetic field is changed.

3.2 Track Reconstruction

The off-line pre-processing of the data includes the reconstruction of the tracks using the space points measured by the telescope [4] .

The measurements of the two perpendicular planes of each telescope module are combined into three-dimensional space points. Track segments are constructed by combining the space points from the most upstream and most downstream modules. The track is then refined by including the space points from the intermediate telescope modules if the distance between the track and the space point is within 50 microns. Events are included if the track contains at least three space points after this cut.

A number of track quality indicators are available to select a sample of tracks with a predefined efficiency and purity. The most important are: the number of space points in the track fit, the χ^2 of the fit, the track gradients with respect to the beam axis, and the efficiency of the anchor module. After applying these cuts, a large fraction of the track statistics remains, while the effect of fake tracks on the efficiency measurement is well below 1 %.

In the H8 beam tests the position where the tracks were incident on each module is interpolated from the telescope hits with a precision of $\sim 5\mu m$ (including the alignment error). The dominant error is due to track multiple scattering within the module array. In the KEK beam tests, with a much lower beam energy, track reconstruction precisions of better than 10 μm can be obtained for the central four modules without a great loss of statistics.

3.3 Event selection

During the beam period a large number of runs [5] are taken with variable operating conditions: discriminator threshold, bias voltage, incidence angle

[4] The cluster information from the telescope modules is available in the DST, so that custom track reconstructions are still possible

[5] The *run* is the smallest unit of data in the beam test. It contains 10.000 to 30.000 events for a fixed set of operation conditions, in particular threshold.

and magnetic field.

The first step in the analysis is the selection of the event sample. To select a sample of clean, unambiguous events, a number of event selection criteria are applied:

- **Single track events**. In a small fraction of events (depending on the beam intensity, generally of the order of 5 %) more than one track is reconstructed from the telescope information due to its relatively long shaping time. As the integration time of the binary modules is much shorter the second track is generally not detected in the binary system. However, to avoid ambiguities, events with more than one telescope track are rejected from the analysis, as are events where no telescope track has been accepted.
- **Track quality**. From the remaining sample, only those events are accepted where the track satisfies the quality criteria. Most analyses require a minimum number of points in the track fit and set maximum values for the χ^2 of the fit and the slopes of the track with respect to the beam axis. In general, a hit close to the track in the anchor module is required. This combination of cuts efficiently removes fake tracks and tracks suffering a large deflection due to multiple scattering. The loss of statistics in this stage depends on the values of the cut, but is in general of the order of 10-30 %.
- **Masked channels**. During the characterisation of the modules a number of faulty channels is masked. Events where the track points to one of these "bad" channels or immediate neighbours are rejected from the analysis. In recent modules the fraction of masked channels is below 1 %. The loss of statistics in this step is therefore small.
- **Time window**. A final cut removes those events where the trigger phase falls outside the optimum window. The window is optimised separately for each module due to variations in signal cable length. This cut is expensive in terms of statistics: for a 10 ns window only 40 % of the events are retained. As only binary hits in one clock time bin are used, this procedure data effectively converts data taken in "ANYHIT" compression into the equivalent of "LEVEL" compression.

4 Results

4.1 Efficiency and noise occupancy

The most important benchmarks for SCT binary module performance are the efficiency and the noise occupancy at the operating threshold. A detector plane is considered efficient if a binary cluster center is located within $100\mu m$ of the *real* track position, as determined by the interpolated telescope track. The

noise occupancy is measured by counting all hits in special flagged events taken in the periods between every accelerator spill during which there is no beam occupancy. As these events are interleaved with beam events the operating conditions are identical. The noise occupancy is defined as the probability to find a hit due to noise in one channel in one clock cycle.

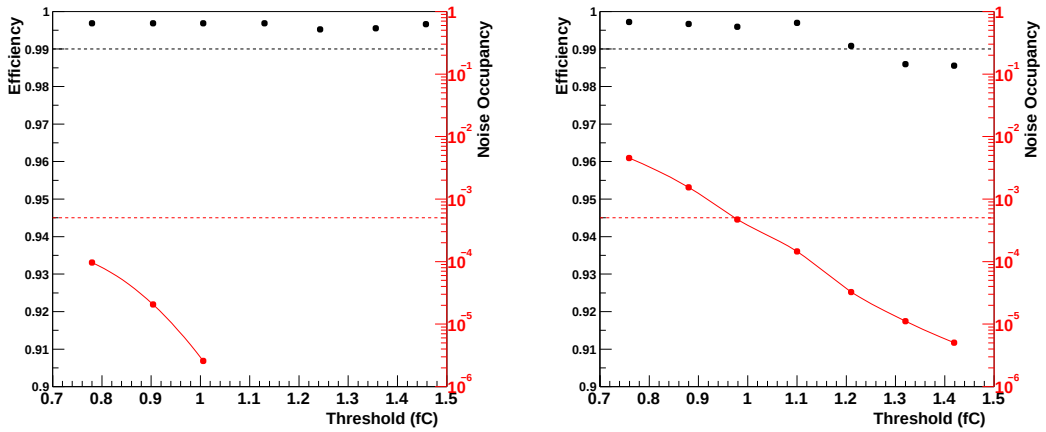

Fig. 2. *Results under the reference conditions of the efficiency* (left axis) *and noise occupancy* (right axis) *versus corrected threshold in fC in the region near the nominal 1.0 fC operating point. The dashed lines indicate the module specifications for efficiency (99 %) and noise occupancy* (5×10^{-4}) *at the nominal operating threshold. The leftmost figure corresponds to a non-irradiated barrel module, the rightmost figure to a module of the same type irradiated to the reference fluence of* $3\times10^{14} p/cm^2$.

Figure 2 shows the efficiency for a number of threshold settings around the envisaged operating threshold of 1 fC. The noise occupancy corresponding to each threshold is shown on the logarithmic axis on the right of the same figure. The results correspond to a non-irradiated barrel module and a module of the same type irradiated up to the reference fluence of $3 \cdot 10^{14}$ p/cm^2. All modules are operated in the same test beam reference conditions: the detector bias voltage is set to 150 V for the non-irradiated modules and to 450 Volts for the irradiated modules, the beam is incident perpendicularly on the modules and no magnetic field is applied.

When the modules are operated with sufficient over-depletion, there is a long plateau where efficiencies over 99 % are obtained. The noise occupancy, on the other hand, is a rapidly falling, nearly Gaussian, function of threshold, independent of bias voltage. The occupancies are found to coincide rather accurately with the expectation from the equivalent noise charges measured during the characterization. After irradiation, the noise occupancy is considerably higher for a given threshold, in agreement with increased noise charge. The efficiency for irradiated modules is seen to fall off at a slightly lower threshold than for similar non-irradiated modules.

The SCT specifications require over 99 % tracking efficiency and a noise occu-

pancy of less than $5 \cdot 10^{-4}$. Both requirements are indicated as dashed lines in the figure. The operating range is defined as the range in thresholds where the efficiency and noise occupancy specifications are both met. For non-irradiated modules, of all four geometrical types, the operating range extends from ~ 0.8 fC up to ~ 1.5 fC. After irradiation, the operating range is significantly narrower for all modules. The lower limits range from 1.0 to 1.2 fC, whereas the upper limit is generally around 1.2 fC.

Silicon micro-strip detectors are discrete measuring devices. In detectors with analog readout the charge on multiple consecutive strips is measured and the position is determined from the properties of the cluster. The clustering procedure yields a quasi-continuous position measurement. In the binary readout scheme, however, the signal in most cases is over threshold on only one strip. Thus, only a discrete measurement is available. This could lead to non-uniformities in the response depending on the position of the track with respect to the two closest strips, particularly in the inter-strip region.

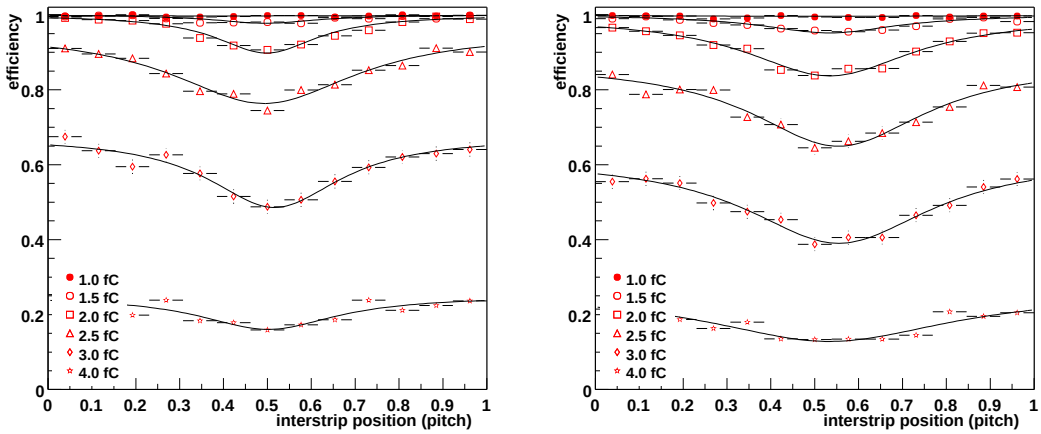

Fig. 3. *Efficiency as a function of the inter-strip position of the incident particle for a non-irradiated (a) and irradiated barrel module (b).*

Figures 3 show the efficiency versus inter-strip position for perpendicularly incident tracks on an irradiated and a non-irradiated barrel module. The position is expressed in units of the read-out pitch: inter-strip position 0.5 corresponds to tracks crossing the detector at equal distances from the two strips and inter-strip positions of 0 and 1 correspond to tracks that are incident on the centre of the readout strip. In the central region diffusion of the charge carriers leads to increased charge sharing. The lower signal on each of the strips is reflected in the reduced efficiency at high threshold. However, at the operating threshold the efficiency is normal. Note that the distribution is smeared by the uncertainty in the position of the interpolated track that becomes significant at this level. The case for non-perpendicular incidence is discussed below.

4.2 Spatial resolution

The spatial resolution is obtained as the width of the residual distribution - the distribution of the difference between the extrapolated track position and the center of cluster [6] .

Typical residual distributions are shown in figure 4. The outline histograms show the result using only single strip clusters: the residuals form a uniform distribution from $-p/2$ to $p/2$, where p is the readout pitch, characteristic for binary readout. The spatial resolution due to single-strip clusters is given by the RMS of a uniform distribution with a width equal to the pitch: $\sigma = p/\sqrt{12} \sim 23\mu m$. The contribution from two-strip clusters is shown in the filled histograms. As the multi-strip clusters predominantly occur in a narrow region in the central region between two strips the resolution of the multi-strip clusters is better than that of single-strip clusters [7] . Note that the residuals are smeared by the error on the interpolation of the telescope tracks, of the order of $5\mu m$.

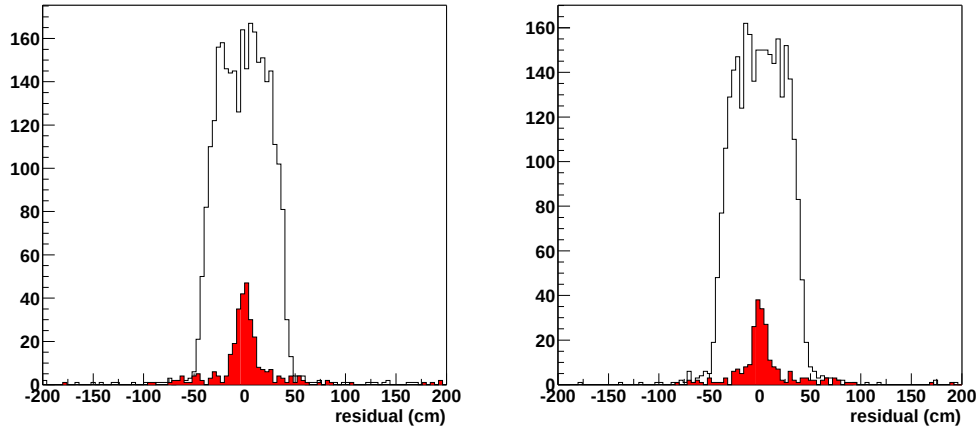

Fig. 4. *Single plane residuals with respect to the position interpolated from the beam telescope measurements. Two modules irradiated to more than* $3 \cdot 10^{14} p/cm^2$*: a barrel module* (left) *and an end-cap outer module* (right). *The discriminator threshold is set to 1 fC. For the end-cap module the residuals have been rescaled to a pitch of* $80\mu m$.

In normal operation the fraction of multi-strip clusters is small and the resolution is close to $23\mu m$, independently of the operating parameters. Also, no significant change is observed in the residuals at a threshold of 1 fC after irradiation. The effect of the bias voltage and the incidence angle on charge sharing are discussed in subsections 4.4 and 4.5, respectively.

[6] For end-cap modules the residuals are projected on the line where the pitch is equal to that in the barrel modules ($80\mu m$) to facilitate comparison

[7] see the discussion in the next section

The residual distribution of figure 4 is a measurement of the spatial resolution of a single detector plane. The stereo angle of 40 mrad between the two detector planes of the SCT module allows the determination of a two dimensional space point. The intersection of two 80 μm wide strips defines a rhomb with short axis $\frac{p}{\cos\alpha/2}$ and long axis $\frac{p}{\sin\alpha/2}$, where p is the readout pitch and α is the stereo angle. The short axis corresponds to the X axis of the global coordinate system in the test beam, while the long axis is identified with the Y axis. Projecting the uniform distribution in the rhomb on both axes yields triangular distributions with an RMS $\sim$ 17 microns in X and RMS $\sim$ 810 microns in Y, see figure 5. More detailed results on the single module resolution are reported in [5].

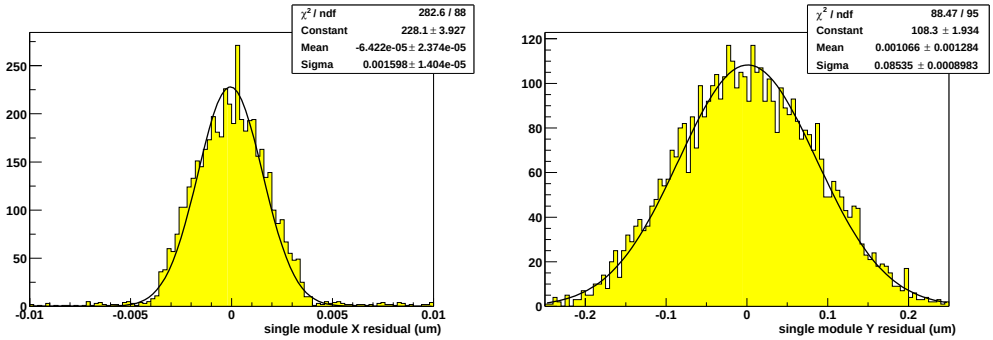

Fig. 5. *Residuals of the space point reconstructed on a single, irradiated barrel module with respect to the position interpolated from the beam telescope measurements: X, perpendicular to the long axis of the module* (left) *and Y, parallel to the long axis of the module* (right). *The discriminator threshold is set to 1 fC.*

4.3 Median charge

In the binary readout scheme, it is necessary to scan the discriminator threshold through the charge distribution in order to reconstruct the full signal distribution. The curve of efficiency as a function of threshold (known as the S-curve) measures the integrated charge distribution. The *collected* charge distribution is described by the Landau distribution of the *deposited* charge convoluted with the Gaussian noise distribution and the effect of charge sharing between neighbouring strips. The median charge is measured as the charge corresponding to the threshold where 50 % efficiency is obtained. In practice, the threshold is expressed in equivalent charge and the value for the median charge is obtained directly from a fit with a skewed error function:

$$\epsilon = \epsilon_{max} f(x \cdot [1 + 0.6\frac{e^{-\epsilon x} - e^{\epsilon x}}{e^{-\epsilon x} + e^{\epsilon x}}]) \quad (1)$$

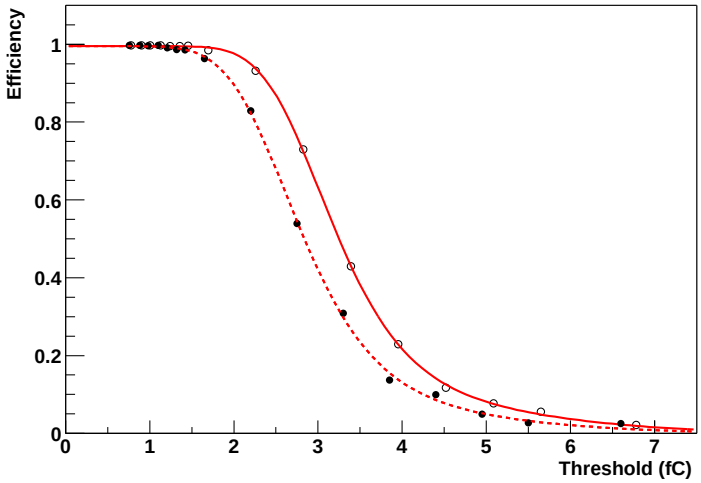

Fig. 6. *Typical efficiency versus threshold* s-curves *for non-irradiated* solid *and an irradiated* dashed *modules run under reference conditions.*

, where f denotes the complementary error function. The median charge μ, the width σ and the maximum efficiency ϵ_{max} are free parameters and $x = (thr - \mu)/\sigma^2$. This parameterisation describes the data quite accurately.

In figure 6 the S-curves of a non-irradiated and an irradiated module are shown for reference operating conditions. Each point corresponds to the efficiency measured on a single run of $\sim$ 15000 events. The lines represent the fit with the function of equation 1.

The error on the median charge is dominated by the uncertainties in the calibration. The variation of the calibration from one chip to the next is evaluated in the beam test by pointing the beam to areas of the detector read out by different chips and measuring the median charge of each chip separately. For non-irradiated modules the chip-to-chip spread in the median charge is of the order of 4%. After irradiation the spread increases to nearly 10% on some modules [2]. Correcting the charge of each chip by measurements of the calibration DAC output improves the uniformity, suggesting that the spread in median charges is due to variations in the components of the calibration circuit [19].

The random error of a single median charge measurement is therefore of the order of 0.1 fC for non-irradiated modules and 0.3 fC for irradiated modules. In practice, comparison between different modules is greatly facilitated by the use of the signal-to-noise ratio, the ratio of median charge and the equivalent noise charge.

The average median charge of a significant number of recent barrel and outer end-cap modules is 3.5 ± 0.1 fC at a bias voltage of 300 Volts. Division of the median charge by the equivalent noise charge, which is measured as part of

the electrical characterization of the module, yields a signal-to-noise ratio of ~ 14. For inner modules the shorter 6 cm strips have a lower capacitive load at the amplifier and therefore an improved noise performance, yielding a S/N of ~ 20.

From a GEANT4 simulation (see for details [3]) of the energy deposition a median charge of 4.0 fC is expected. The observed median charge is clearly lower. Less than 0.1 fC of this difference can be attributed to the measurement procedure, indicating a discrepancy between the deposited and collected charge.

Charge shared between neighbouring strips cannot be re-clustered in the binary readout scheme as it is predominantly below threshold. The effect of different charge sharing mechanisms on the median collected charge sharing is investigated in reference [3]. Diffusion of the charge carriers while they drift toward the readout plane can be studied using the position predicted by the telescope. Test beam measurements indicate that the loss of median charge due to diffusion is 0.13-0.16 for all module types. Cross-talk between neighbouring channels is expected to be responsible for a charge loss of 6%, i.e. ~ 0.26 fC. Finally, the charge carried to neighbouring strips by δ-electrons can be quite substantial. However, GEANT4 model calculations show that even though this effect leads a less pronounced high-energy tail in the charge distribution, the median charge is not significantly affected.

The total charge loss due to the three charge sharing mechanisms is thus expected to amount to ~ 0.4 fC. Thus, charge sharing accounts for most of the discrepancy between the observed median charge, 3.5 fC, and the expected charge deposition, 4.0 fC.

4.4 Detector Bias Voltage

The bias voltage of the detector is an important operating parameter. For irradiated detectors the signal grows with increasing bias voltage. The maximum voltage is limited by the detector breakdown voltage (greater than 500 Volts for SCT detectors), the limit of the power supplies (450-500 Volts) and the limit imposed by the cooling system. Therefore, a good characterisation of the performance versus detector bias voltage is essential.

Figure 7 shows the dependence of the signal-to-noise ratio on the detector bias voltage for three modules. For the non-irradiated module, the median signal-to-noise ratio is nearly constant, S/N ~ 13, above 150 V. The charge difference between 150 V and the highest voltage, 300 V, is 0.15 fC. As the bias voltage is decreased towards the depletion voltage (around 75 Volts in these detectors) the signal gradually decreases. This can be explained as a ballistic deficit

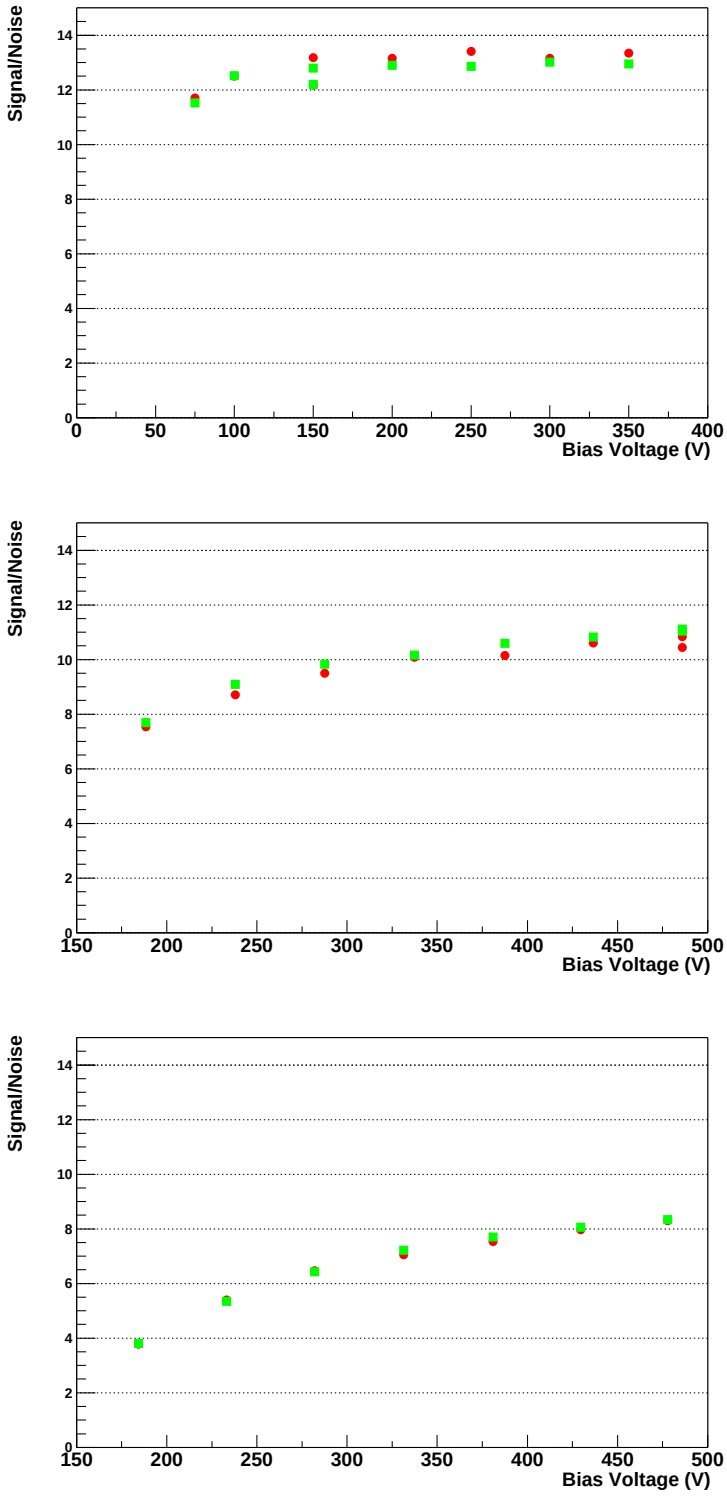

Fig. 7. *Median signal-to-noise ratio versus bias voltage. Top figure: non-irradiated barrel module. Central figure: irradiated barrel module. Bottom figure: irradiated endcap outer module.*

of the shaper circuit, i.e. the integration window of the front-end electronics is no longer large compared to the charge collection time of the detector, leading to charge loss. The drift time of the holes becomes comparable to the peaking time of the shaper at a bias voltage of around 100 Volts. For a detailed discussion of charge collection times, see references [20,21].

The relation between signal and bias voltage for irradiated modules is more complicated. The collected charge does not saturate at any voltage up to the maximum available in the beam test, 500 V [8]. The depletion voltage is estimated to be around 250 V for these detectors. The maximum value of the charge at 500 V approximates the charge found in the non-irradiated modules. Due to the increased noise, the signal-to-noise ratio of modules irradiated to a fluence of $3 \cdot 10^{14} p/cm^2$ reaches only about 7-11. The large spread between modules is not completely understood but may partly be due to dose uncertainty.

Various possible explanations exist for the high over-depletion needed to reach full charge collection. Measurements by the ROSE collaboration [22] indicate that there is considerable charge loss due to trapping of the charge carriers in radiation-induced lattice defects. Assuming a constant trapping probability per unit time, the effect is bias voltage dependent through the charge collection time. For small over-depletion, the different field distribution across the silicon in type-inverted bulk material may lead to a ballistic deficit of the shaper.

In irradiated, type-inverted p^+n detectors the junction forms at the backplane, between the n^+ material of the backplane and the p-bulk. Thus, if the bias voltage is lower than the depletion voltage the depleted region does not reach the readout side of the detector. A small signal is nevertheless induced on the strips across the dead region.

4.5 Incidence angle & magnetic field

In ATLAS the SCT modules will be subject to a 2 Tesla magnetic field. Also, tracks will not generally be perpendicularly incident on the detector plane. Therefore, an important subject of study is the influence of the magnetic field and incidence angle on the performance of the modules.

In the August 2001 beam test [5] threshold scans were performed at various angles, both without magnetic field and in the 1.56 Tesla field of the Morpurgo magnet. In this section the dependence of the most important parameters

[8] The actual bias voltage on the silicon is lower than the supply voltage by up to 30 V due to the voltage drop in the hybrid bias resistor.

- efficiency at the operation threshold, median collected charge and spatial resolution - on the incidence angle and field is discussed.

Two orientations should be considered. The incidence angle in the detector R-z plane is determined by the detector geometry. It becomes quite large (68^o) for the outermost modules on the inner barrel. The longer path length through the silicon leads to an increase of the median charge with $1/\cos(\alpha)$. This behaviour has been confirmed in beam tests up to angles of $\sim 16^o$ in 2001 [5] and in a second measurement at $\sim 35^o$ in 2002 [2](see the leftmost figure 8)

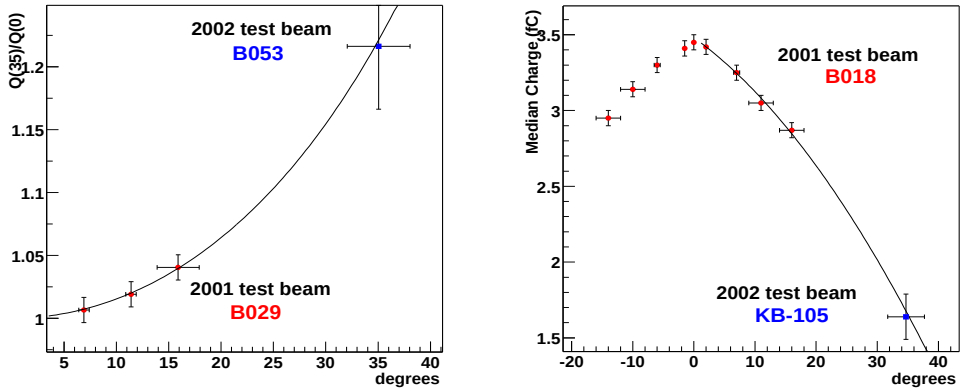

Fig. 8. *Leftmost figure: Median charge versus incidence angle in the $R-z$ orientation. The points are normalised with respect to the 0^o result. The plot is fitted with the function $1/\cos\alpha$ as expected from the increased path length. Rightmost figure: Median charge and incidence angle in the $R-\phi$ plane. In both figures, the 35^o point is a result from the 2002 test beam, while the other measurements refer to a barrel module measured in 2001. The detector bias voltage is 150 V.*

The incidence angle in the $R\phi$ plane is due to the deflection of particles in the solenoidal magnetic field. It is generally small: for a 1 GeV particle the incidence angle is of the order of $\sim 10^o$. The tilt angle of the barrel modules forms an offset of 7^o. The longer path length again leads to a small increase of the signal. But, in this orientation the projection of the particle trajectory on the readout plane is perpendicular to the readout strips. For large incidence angles the projected distance becomes significant compared to the pitch and charge sharing between neighbouring strips becomes important. The net effect is a decrease of the median collected charge, as shown in the rightmost figure of 8.

In a strong magnetic field the Lorentz force deviates the drifting carriers. Figure 9 shows how the Lorentz force is equivalent to a rotation by a small angle $\Theta_L = \mu^H B = r_H \mu B$, where μ^H the Hall mobility, the conduction mobility μ multiplied by the Hall scattering factor r_H [23].

In the August 2001 beam test the combined effect of incidence angle and

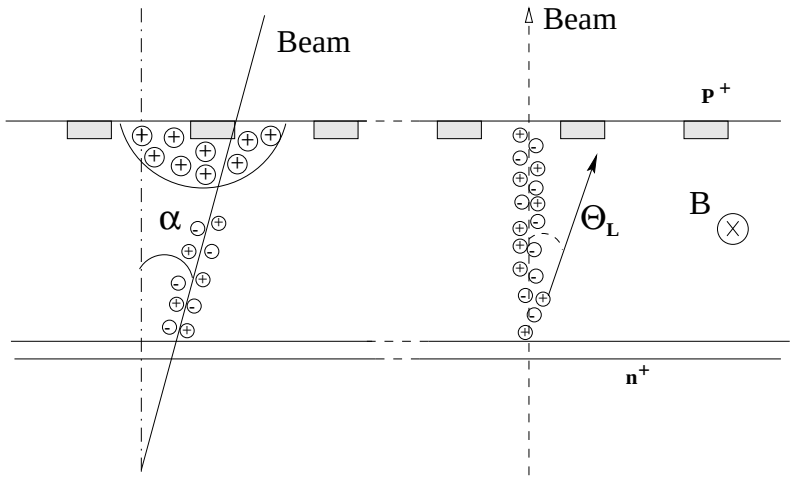

Fig. 9. *Representation of the effect of the incidence angle and the application of a magnetic field.*

magnetic field was studied in an orientation representative for barrel modules at $\eta = 0$. The modules are biased to nominal bias voltages: 150 Volts for non-irradiated modules, and 350 Volts after the full expected dose. The modules are naturally classified in two groups: irradiated and non-irradiated modules. The results are presented as averages over all (non-) irradiated barrel modules, the errors representing the variation between different modules.

A sensitive measure of charge sharing is the average cluster size. Here, the cluster size dependence on angle in a magnetic field is used to determine the Lorentz angle. Noise clusters are excluded by placing a 200 μm window around the track position predicted by the telescope. Figure 10 shows the average cluster size as a function of incidence angle (filled markers). The open markers show the same measurement in a 1.56 T magnetic field.

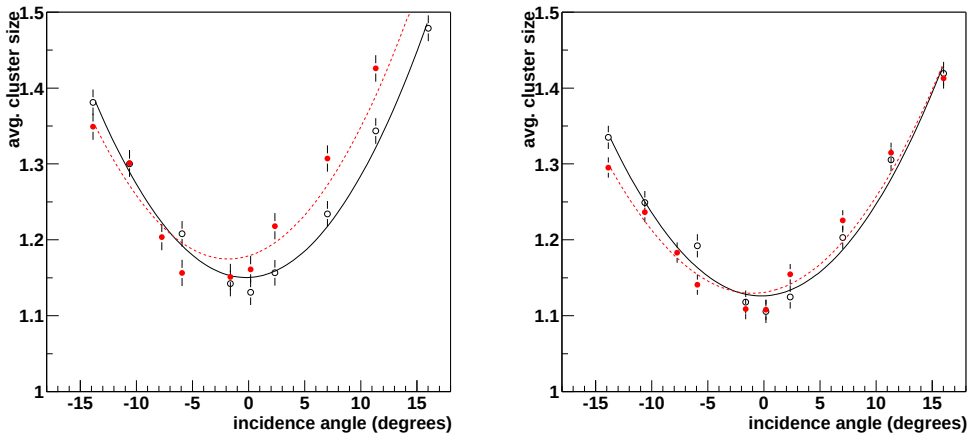

Fig. 10. *Cluster size versus angle for non-irradiated modules at 1 fC (left) and irradiated at 1 fC (right). Filled markers are measurements with a magnetic field of 1.56 T, the open markers without field*

The increase of cluster size at non-perpendicular incidence reflects the increased charge sharing. The effect of the magnetic field is a shift of the distribution by a few degrees.

The Lorentz angle is determined as the minimum of the cluster size versus angle curve. The measurements from all modules in both groups have been combined. The statistical error is taken to be the standard deviation of the measurements of a group. As a cross check, the fit results for data taken without magnetic field have been calculated. The result $\Theta_0 = 0.4^\circ \pm 0.2^\circ$ reflects the overall uncertainty in the angle scale. The Lorentz angle obtained for both groups, non-irradiated and irradiated modules, is then:

$$\Theta_L(150V) = 3.3^\circ \pm 0.3^\circ \tag{2}$$

$$\Theta_L(350V) = 2.1^\circ \pm 0.4^\circ \tag{3}$$

As the irradiated modules are biased at a higher voltage, the observed difference could be due to an electric field dependence of the Lorentz angle or a change in the properties of the charge carriers due to irradiation. In the literature, the effect of proton irradiation on the mobility and thus Lorentz angle of holes is found to be compatible with no effect [20,24,25]. The difference in voltage, i.e. the electric field inside the detector, has an effect on Θ_L through the electric field dependence of the carrier mobility μ. Theoretical models[23,24] applied to beam test conditions (silicon temperature $T = 261^o$ K, thickness $d = 285\mu$m and field $B = 1.56$ T) predict values of $\Theta_L(150\text{V}) = 3.3^\circ$ and $\Theta_L(350\text{V}) = 2.4^\circ$. The predictions agree within errors with our measurements.

In the range of angles $[-14^o, 16^o]$ studied in the beam test no significant effect on the efficiency is observed at a threshold of 1 fC. For irradiated modules a small effect becomes visible when the discriminator threshold is raised to 1.2 fC. Still, the efficiency is over 97 % for all angles.

As discussed in section 4.2 the spatial resolution with binary readout depends on the number of strips in the cluster. An increase of multi-strip clusters is expected to lead to a better resolution. In figure 11 the effect of the incidence angle on the spatial resolution of non-irradiated (leftmost figure) and irradiated modules (rightmost figure) is shown. The difference between the worst (0°) and the best ($\pm 15^\circ$) resolution is around 2 μm. Again the magnetic field causes a shift.

The deviation of the drifting carriers due to the Lorentz effect leads to a shift of the apparent position by several μm. A good description of the bias voltage dependence of the Lorentz angle allows for a precise correction of this effect.

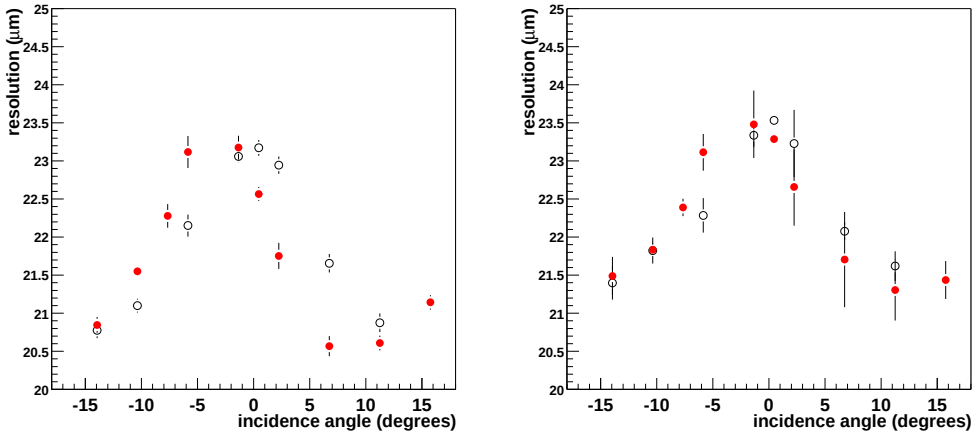

Fig. 11. *Resolution in μm versus angle for non-irradiated modules at 1 fC (left) and irradiated at 1 fC (right). Filled marker are measurements in a 1.56 T magnetic field, open markers without field*

5 Conclusions

Repeated test beams of ATLAS SCT modules have yielded a wealth of information on the performance of a binary readout scheme for silicion micro-strip detectors. The measurements discussed here demonstrate that the various geometrical types satisfy the ATLAS efficiency and noise specifications. The measured spatial resolution is in agreement with the $p/\sqrt{12}$ expectation for single strip clusters.

For the reference detector bias voltage of 150 V, the charge collection efficiency is over 95 %. Modules of the barrel and end-cap types show similar charge collection results. An analysis of the charge loss mechanisms in the binary readout scheme explains the difference between the measured median *collected* charge and the (GEANT4) expectation for the median *deposited* charge. The median signal-to-noise ratio of modules with 12 cm detectors is ~ 14. For the shorter inner modules the improved noise performance leads to a $S/N \sim 20$.

Modules irradiated to $3\times10^{14}p/cm^2$ collect about 90 % of the deposited charge when biased to 350 V. The noise increases significantly as a result of the irradiation. The median signal-to-noise ratio decreases to values in the range 7-11. The reduced signal-to-noise ratio leaves a rather narrow operating range where the efficiency (> 99 %) and noise occupancy ($< 5 \cdot 10^{-4}$) specifications are met.

The deviation of drifting charge carriers in a magnetic field has been measured on several modules. For a 1.56 T magnetic field and a detector bias voltage of

150 V a Lorentz angle of $3.3^o \pm 0.3^o$ is found. At higher voltage the Lorentz angle decreases significantly: $\theta_L = 2.1^o \pm 0.4^o$ at 350 V. The measurements are in good agreement with the model of reference [23].

Importantly, the performance of SCT modules is - to a large extent - understood. Beam test results have been incorporated into the *digitisation* of the GEANT4 simulation of the the ATLAS detector [26]. A realistic description of the bias voltage and incidence angle dependence of the response is implemented for non-irradiated modules. The model is currently being updated using more recent beam test data [27].

References

[1] P.J Dervan et al. Irradiation of ATLAS SCT Modules and Detectors in 2002. *ATLAS Internal Note*, ATL-INDET-2003-001.

[2] J.E. Garcia Navarro et. al. Beamtests of ATLAS SCT modules in 2002. *ATLAS Internal Note in preparation*, 2003.

[3] M.Vos et. al. Charge collection with binary readout. *ATLAS Internal Note*, ATL-INDET-2003-011.

[4] M.Vos et. al. A study of the tracking performance of irradiated SCT prototypes using test beam data. *ATLAS Internal Note*, ATL-INDET-2003-003.

[5] A. Barr et. al. Beamtests of ATLAS SCT modules in august and october 2001. *ATLAS Internal Note*, ATL-INDET-2002-024.

[6] Y. Unno et. al. Beamtest of non-irradiated and irradiated ATLAS SCT microstrip modules at KEK. *IEEE Trans. Nucl. Sci.* 49 (2002) 1868–1875.

[7] J. Bernabeu et. al. Beam study of irradiated ATLAS-SCT module prototypes. *Nucl. Instrum. Meth.*, A 485 (2002) 67–72.

[8] A. Barr et. al. Beamtests of ATLAS SCT modules in june and august 2000. *ATLAS Internal Note*, ATL-INDET-2002-005.

[9] J. Bernabeu et. al. Results of the 1999 H8 beam tests of ATLAS-SCT prototypes. *ATLAS Internal Note*, ATL-INDET-2000-004.

[10] A. Akimoto et. al. Results of the 1999 H8 beam tests of ATLAS-SCT prototypes. *Nucl. Instrum. Meth.*, A 466 (2001) 397–405.

[11] F. Albiol et al. Beam test of the ATLAS silicon detector modules. *Nucl. Instrum. Meth.*, A 409 (1998) 236–239, .

[12] F. Albiol et al. Beam test of the ATLAS silicon detector modules with binary readout in the cern h8 beam in 1996. *ATLAS Internal Note*, ID-96-153, 1996.

[13] F. Albiol et al. Beam test results on a prototype SCT module using csem detectors. *ATLAS Internal Note*, ID-96-153, 1996.

[14] J. deWitt et al. Beam test of the binary silicon system in h8 in september 1995. *ATLAS Internal Note*, ID-96-135, 1996.

[15] H. F. W. Sadrozinski et al. Monitoring the performance of silicon detectors with binary readout in the ATLAS beam test. *Nucl. Instrum. Meth.*, A383:245–251, 1996.

[16] L.Eklund and P.W.Phillips. Electrical tests of sct hybrids and modules.

[17] M. Mangin-Brinet et al. Electrical test results from ATLAS-SCT end-cap modules *ATLAS Internal Note*, ATL-INDET-2003-004.

[18] ABCD3T ASIC Project Specification Version 1.1

[19] The SCT end-cap collaboration. Final design report of the end-cap module. *ATL-IS-EN-009*, 2002.

[20] T.J. Brodbeck et. al. Carrier mobilities in irradiated silicon. *Proceedings of 5th Conference on Position Sensitive Detectors, London, September 1999*, ROSE/TN/2000-09.

[21] L.J. Beattie et. al. The electric field in irradiated silicon detectors. *Nucl. Instrum. Meth.* A 418 (1998) 314-321.

[22] G. Lindstrom F. Lemeilleur and S. Watts. Third RD48 status report. CERN-LHCC-2000-009.

[23] T. Lari et. al. Lorentz angle variation with electric field for ATLAS silicon detectors. *ATL-INDET-2001-004*, 1998.

[24] V. Bartsch et. al. An algorithm for calculating the lorentz angle in silicon detectors. *CMS IN-2001/027*, 2001.

[25] V. Eremin and Z. li. *Nucl. Inst. and Meth.* A 362 (1995), 338.

[26] S. Gadomski. Model of the SCT detectors and electronics for the ATLAS simulation using geant4. *ATLAS internal note*, ATL-SOFT-2001-005.

[27] P. Reznicek. *Test of semiconductor microstrip detectors of ATLAS detector.* PhD thesis, Charles University of Prague, 2003.